

Growth and characterization of ZnS nanofilms grown by RF magnetron sputtering on GaAs

J. Díaz-Reyes, R. Castillo-Ojeda, J. Martínez-Juárez, O. Zaca-Moran, J. E. Flores-Mena, and M. Galván-Arellano

Abstract—Zinc sulphide (ZnS) is one of the most important II-VI group semiconductors, with a wide direct band gap of 3.8 eV has been extensively investigated and used in electroluminescent devices, flat panel displays, infrared windows, sensors, and lasers. To explore the possibility of using it in electroluminescent devices, a study of the structural and optical properties of the host material is an important step. Based on the above criterion, the structural and optical properties of ZnS nanofilms have been studied in the present work. ZnS nanofilms were grown on (001) GaAs substrates at different temperatures by RF magnetron sputtering. The ZnS chemical stoichiometry was determined by Energy-dispersive X-ray spectroscopy (EDS). The XRD analysis and Raman scattering reveal that ZnS deposited nanofilms showed hexagonal wurtzite crystalline phase. The average crystallite size range of the film was from 8.15 to 32.95 nm, which was determined using the Scherrer equation. Besides an experimental study on first- and second-order Raman scattering of ZnS films is made. An energy level diagram involving oxygen traps and interstitial sulphur ions used to explain the origin of the observed emission peaks in the room temperature photoluminescence spectra.

Keywords—II-VII semiconductor compounds, hexagonal wurtzite-type ZnS, X-ray diffraction, SEM-EDS, photoluminescence, Raman Sputtering.

I. INTRODUCTION

WIDEband gap semiconductors containing a great number of defects, surface states or doped with optically active

J. Díaz-Reyes is with Center of Applied Biotechnology Research, National Polytechnic Institute. Ex-Hacienda de San Juan Molino Km 1.5. Tepetitla, Tlaxcala. Zip code 90700. México (Phone: 52 (248) 4 87 07 65; Fax: 52 (248) 4 87 07 66; e-mail: joel_diaz_reyes@hotmail.com).

R. Castillo-Ojeda is with the Polytechnic University of Pachuca. Km. 20, Rancho Luna, Ex-Hacienda de Santa Bárbara, Municipio de Zempoala, Hidalgo. Zip code 43830. México (e-mail: rcastillo_ojeda@yahoo.com.mx).

J. Martínez-Juárez is with the Research Center of Semiconductor Devices, Meritorious Autonomous University of Puebla. Av. San Claudio y 14 Sur, Ciudad Universitaria, Puebla. Zip code 72570. México (email: javmartinez11@gmail.com).

O. Zaca-Moran is with Center of Applied Biotechnology Research, National Polytechnic Institute. Ex-Hacienda de San Juan Molino Km 1.5. Tepetitla, Tlaxcala. Zip code 90700. Mexico (e-mail: orlandozaca@hotmail.com).

J. E. Flores-Mena is with the Faculty of Electronic Science, Meritorious Autonomous University of Puebla. Av. San Claudio y 18 Sur, Ciudad Universitaria, Puebla, Puebla. Zip code 72570. Mexico (email: eflores@ece.buap.mx).

M. Galván-Arellano is with Section of Solid State Electronics, Department of Electrical Engineering, Research Center and Advanced Studies, National Polytechnic Institute. Av. Instituto Politécnico Nacional 2508, Col. Zacatenco, Gustavo A. Madero. México, D. F. 07360. México (e-mail: miguel_galvan_2013@yahoo.com).

luminescence centres, have created new opportunities for optical studies and development of applications. ZnS is an important wide band gap semiconductor which continues to gain in recent years in view of its application potential in optoelectronic devices such as light emitting diodes, flat panel displays, nonlinear optical devices, sensors, lasers and photocatalysis [1,2]. Deep-level energy bands allow semiconductor materials to emit at longer wavelengths. Then it is possible to fabricate LEDs from these materials [3]. Nevertheless for some uses, it has been shown that such materials must be grown with a monocrystalline structure and a smooth surface [4]. Zinc sulphide (ZnS), an important semiconductor compound of the IIB-VI groups, is mostly found in one of two structural forms cubic sphalerite or hexagonal wurtzite, which have wide band gaps of 3.54 eV and 3.80 eV, respectively at 300 K [5]. It is a well-known luminescent material having prominent and promising applications in displays, sensors and blue-light emission device application [6]. The II-VI semiconductor ZnS is used in many applications primarily for its luminescent properties. It has a direct band gap of 3.8 eV and a small exciton Bohr radius of 2.5 nm. Owing to its wide band gap, it is used in violet and blue regions.

ZnS has been grown on Si and GaAs substrates [6,7]. It is closely lattice matched with Si (0.2%), which makes it a promising material for the integration in optoelectronic devices on Si substrates. However, ZnS and Si exhibit a large thermal expansion coefficient mismatch (13.6%) while the thermal expansion coefficients of ZnS and GaAs are better matched (10.5%). Furthermore, ZnS and GaAs exhibit a large lattice constant mismatch (4.5%). Growth of ZnS thin films has been conventionally done using several methods, such as chemical vapour deposition (CVD) [8], molecular beam epitaxy (MBE) [9], atomic layer epitaxy (ALE) [10], metallorganic chemical vapour deposition (MOCVD) [11], successive ionic layer adsorption and reaction methods (SILAR) [10], metallorganic vapour phase epitaxy (MOVPE) [12], pulsed laser deposition (PLD) [13] and electron induced epitaxy (EIE) [7].

The main advantage of the nanostructures is their size dependent property. As the size approaches that of the Bohr radius, quantum confinement effects result in the blue shifting of the band gap [3]. The Bohr radius of ZnS is 2.5 nm [14]. In this paper, the diameter of ZnS nanofilms is 8.15–32.95 nm, which is much larger than the Bohr radius as well as the excitonic diameter. Therefore, the quantum confinement effect may not be significant in these nanostructures. The recombination properties of the ZnS nanofilms differ from

those of bulk ZnS due to the larger surface to volume ratio. With reduction in size, the surface area plays a dominant role in the material properties, and the presence of many surface defects may also affect the emission properties of ZnS nanostructures.

Recently, it has been used rf magnetron sputtering to grow a variety of materials including GaAs, Ge, Si and some other combinations of them [15]. This technique can deposit large area films of well-controlled compositions economically and the growth rate is high enough for thick films and low enough for ultrathin films by changing the sputtering time [16]. In the present work, we report the growth and characterization studies of ZnS thin films on GaAs (001) deposited at various temperatures (180–630°C) using an rf planar magnetron sputtering system. Effects of temperature during the sputtering with Ar-plasma on crystalline quality, particle size and morphology of the thin films were studied by SEM-EDS, X-ray diffraction, Raman spectroscopy and room temperature photoluminescence. Raman and photoluminescence spectroscopy are powerful and non-destructive optical tools to study vibrational and optical properties of ZnS nanostructures. ZnO is a Raman active material with a hexagonal wurtzite structure that belongs to the space group C_{6v} (6 mm).

II. EXPERIMENTAL DETAILS

The used substrates were (100) GaAs semi-insulating doped with chromium of $10 \times 10 \text{ mm}^2$ of area, with 50 mm separation between the target and substrate. The direct growth of ZnS on GaAs substrates is advantageous because of not only it reduces the polar–nonpolar interface problems but also the thermal expansion coefficients are matched. The base pressure inside the chamber was lower than 7.5×10^{-7} mbar. Plasma of Ar (99.999%) was created to sputter a 100 mm diameter, water-cooled, ZnS (99.99%) target mounted under a planar magnetron. The RF power was 50 W. The sputtering time was about 2.0 h for all deposited samples. During sputtering process the Ar-pressure was maintained at 15×10^{-3} mbar. A partial pressure of hydrogen gas was introduced to the growth chamber during 30 min at room temperature before thin film deposition on the GaAs substrate. This gas partial pressure condition was maintained during the temperature ramp from room temperature to the growth temperature. Grown samples are listed in Table I. The crystalline phase and structure of the films was determined with a Bruker D8 Discover diffractometer using the copper $K\alpha$ radiation ($\lambda=1.5406 \text{ \AA}$) at 40 kV and 40 mA with parallel beam geometry. Raman scattering experiments were performed at room temperature using the 6328 \AA line of a He-Ne laser at normal incidence for excitation. The laser light was focused to a diameter of 6.0 \mu m at the sample using a 50x (numerical aperture 0.9) microscope objective. The nominal laser power used in these measurements was 20 mW. Scattered light was analyzed using a micro-Raman system (Lambram model of Dilor), a holographic notch filter made by Kaiser Optical System, Inc. (model superNotch-Plus), a 256×1024 -pixel CCD used as detector cooled to 140 K using liquid nitrogen, and two interchangeable gratings (600 and 1800 g/mm). Typical spectrum acquisition time was limited to 60 s to minimize the sample heating effects. Absolute spectral feature position

calibration to better than 0.5 cm^{-1} was performed using the observed position of Si which is shifted by 521.2 cm^{-1} from the excitation line. Room-temperature photoluminescence was taken with a solid state laser 325 nm with 60 mW as excitation source and a SCIENCETECH 9040 monochromator was used to perform the sweep of wavelength at room and low temperature in a CRYOGENICS cryostat.

III. EXPERIMENTAL RESULTS AND DISCUSSION

Figure 1 shows XRD diffractograms from some of the polycrystalline ZnS nanostructures grown on GaAs (001). It is observed from XRD patterns that ZnS films deposited even at low temperature are in crystalline nature, which present two peaks dominant at 31.59 and 65.94° . This may be attributed to the fact that the crystalline GaAs substrate facilitates the growth of crystalline ZnS thin films and their crystal lattice orientation is initiated on the GaAs substrates at room temperature. It can be seen that each peak corresponds fairly well with data of ZnS marked in the software DICVOL04 data. The obtained structural parameters with the software DICVOL04 data are in good agreement with the published ones. From this close agreement, it is confirmed that as-deposited ZnS films for all the grown temperatures belong to the wurtzite crystal system. The X-ray pattern of as-deposited ZnS film is described in the C_{6v} (6mm) and whose lattice parameters were calculated using the software DICVOL04, obtaining the following lattice parameters values: $a = 3.81 \text{ \AA}$ and $c/a = 1.62$, which are in agreement with the reported values [9]. In all cases the samples present the same reflections and some of them can be assigned. There is a peak highly intense from the ZnS/GaAs nanostructures at 65.94° , which is composed by two peaks that correspond to the wurtzite hexagonal (104) reflection of ZnS and zincblende (004) GaAs reflection that comes from the substrate material, as will be discussed below.

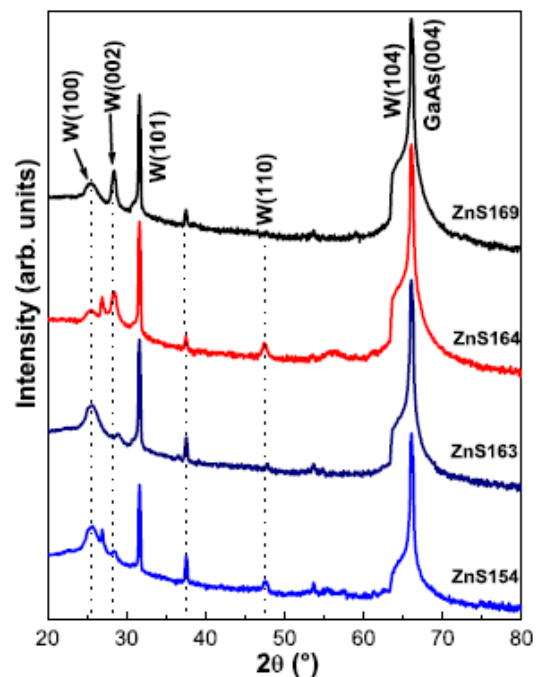


Fig. 1. X-ray patterns of the ZnS films synthesized by RF magnetron sputtering.

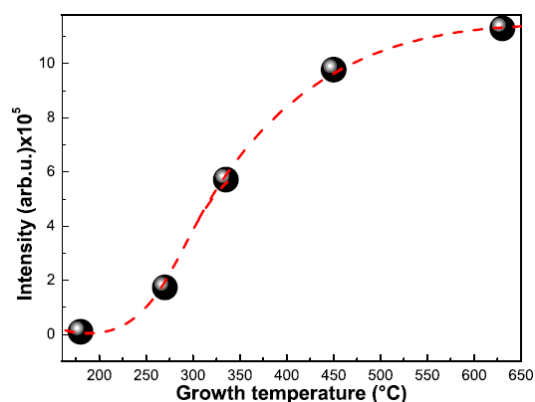


Fig. 2. (004) GaAs peak intensity obtained from X-ray patterns versus growth temperature.

As is observed from the X-ray diffractograms the intensity of the peaks clearly increases as the grown temperature is increased, in particular the peak at 65.94° of sample ZnS169 that is seven orders of magnitude higher compared to ZnS154 as can see in Fig. 1. Fig. 2 shows the zinblende (004) GaAs reflection intensity as a function of the growth temperature. It suggests that the films ZnS154 and ZnS163 are lightly less preferentially oriented than the samples that the ZnS164 and ZnS169. Other peaks are observed on the diffractograms of the samples. The hexagonal (101) reflection is identified at 31.74° , hexagonal (002) reflection is observed at 28.45° and hexagonal (100) at 25.3° . It is clear that increasing the temperature improves the crystalline structure in thin films [17], since main peak increases as the grown temperature is increased, which implies that the crystallinity is better as previously mentioned. Some authors have reported that low growth temperature ($<335^\circ\text{C}$) the ZnS films result in a cubic structure for the thin films [18], but in this case did not occur and all nanostructures were wurtzite type. In order to obtain more structural information, the mean grain size (D) of the deposited nanofilms was evaluated using the Scherrer equation [19]. The mean grain size was calculated from hexagonal (101) reflection of ZnS for the all the samples. The mean grain sizes of the nanostructures are presented in Table I. These results show that the grain size remained almost constant (~ 29 nm) for the temperature range from 180 to 450°C , to higher temperatures the grain size diminishes as can be observed in Table I. Besides, in Table I shows the nanofilms thicknesses grown by rf-sputtering.

TABLE I. RESULTS OF THE ANALYSIS BY EDS OF THE GROWN SAMPLES BY RF MAGNETRON SPUTTERING. BESIDES, IT PRESENTS THE THICKNESSES OF THE NANOFILMS STUDIED IN THIS WORK AND THE GRAIN SIZE OF THEIR ZNS NANOPARTICLES CALCULATED FROM HEXAGONAL (101) REFLECTION OF ZNS.

Sample	T_G ($^\circ$)	S atomic percentage (%)	Zn atomic percentage (%)	Films thickness (nm)	Size grain by XRD (nm)
ZnS140	180	50.21	49.79	865.3	28.18
ZnS154	270	49.01	50.99	845.8	31.95
ZnS163	335	47.07	52.93	887.1	28.31
ZnS164	450	38.89	61.11	828.3	30.30
ZnS169	630	32.18	67.18	801.2	8.15

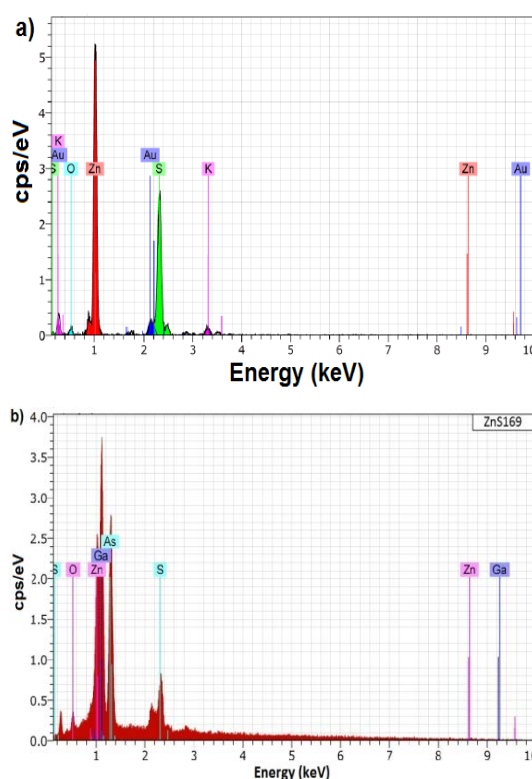


Fig. 3. Bulk EDS spectra of ZnS typical samples: a) ZnS154 and b) ZnS169 samples. The spectra indicate that besides Zn and S, the samples contain a significant amount of oxygen.

The composition of the samples is analysed by EDS, which besides allows to know the presence of any unintentional impurities. The EDS spectra indicate the presence of oxygen in the samples along with zinc and sulphur, see Fig. 3. By XPS analysis has showed that oxygen ions are present in the sample in the form of O^{2-} ions [20] that may produce ZnO. The chemical route for the oxidation reaction of ZnS to ZnO can be represented as $2\text{ZnS} + 3\text{O}_2 \rightarrow 2\text{ZnO} + 2\text{SO}_2$. Oxidation of ZnS to ZnO occurs at high temperatures such as 550°C and 600°C is already reported by many groups [21,22]. Since the temperature during synthesis and air drying in the present case is low, this conversion may have happened only at a very low percentage so that the presence of ZnO could not be detected in XRD. However, these oxygen ions can form trap levels in the band gap, resulting in several transitions contributing to luminescence. Thus, it appears that oxygen has replaced sulphur at a few random points of the ZnS lattice. Figure 3a shows the bulk-EDS spectra of the ZnS nanostructure grown at 270°C . The EDS spectrum indicates that besides Zn and S, the samples contain a significant amount of potassium, gold and oxygen. Fig. 3b shows the typical bulk-EDS spectrum of the sample ZnS sample grown at 630°C . This sample contains a large amount of arsenic and gallium, besides a significant amount of oxygen that allows forming the ZnO. The results of such measurements for the zinc and sulphur are shown in Table I. From these results it is observed that the sample ZnS154 is the one that has a good stoichiometric compound and that starting from it a higher temperature gives a greater presence of zinc in the material and an absence of sulphur. Continuing with the consideration that each unit cell contains

two zinc atoms and two sulphur atoms, then when a stoichiometric deviation of ideal unit cell occurs it could establish a correspondence between vacancies or interstices of some of the elements (V_S , V_{Zn} , Zn_i , S_i). From Table I one observes that the sample ZnS169 contains a lower sulphur concentration, which indicates that it has a higher structural defects concentration.

Figure 4 shows the surface morphology of some typical samples, as is observed in the different figures, the surface morphology depends strongly on the growth temperature, at lower temperature forms some nanostructures as the indicated in Fig. 4a and as the temperature increases these nanostructures diminish indicating that the particle size decreases as has been found by X-ray dispersion. Fig. 5 shows the ZnS164 thickness measured by SEM, which gives a mean value of 828.3 nm.

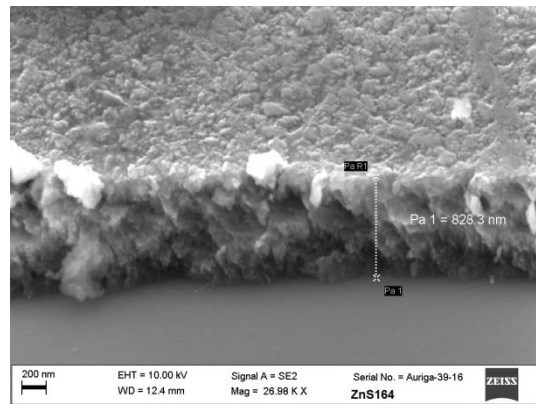


Fig. 5. It shows the thickness of the ZnS164 samples measured by SEM, which was grown at 450°C.

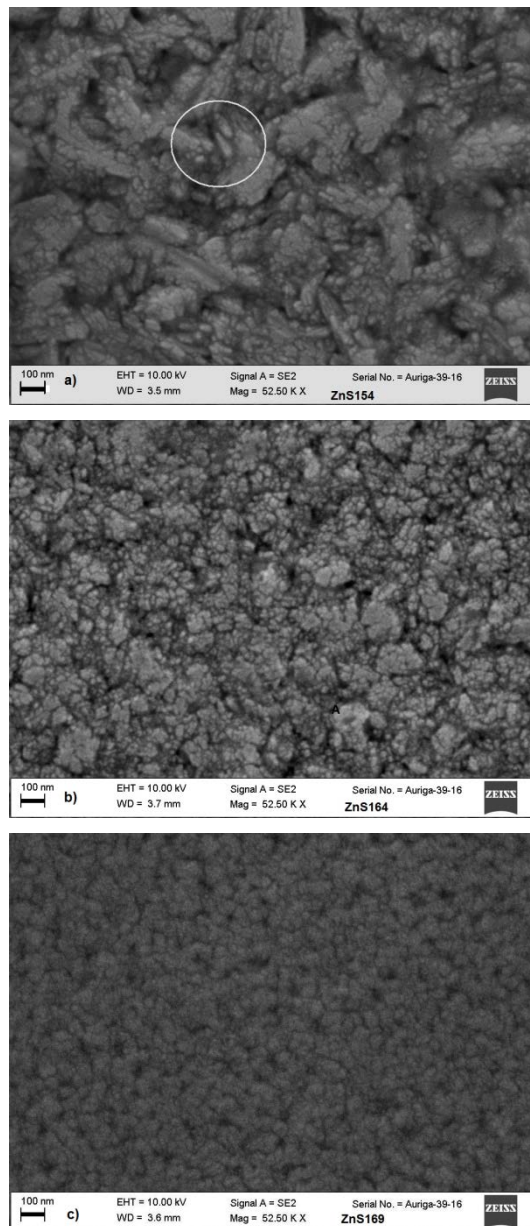


Fig. 4. SEM images of ZnS nanostructures samples with growth temperature: (a) 270°C, (b) 450°C and (c) 630°C.

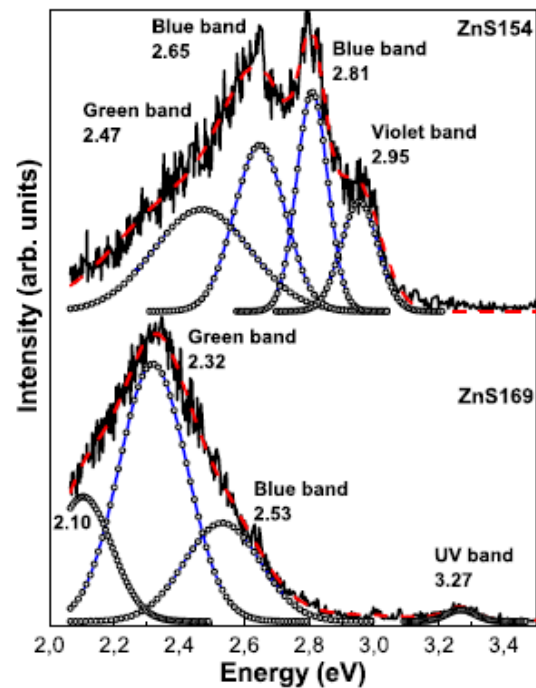


Fig. 6. Room-temperature photoluminescence spectra of the samples: a) ZnS154 and b) ZnS169.

Figure 6 illustrates the room temperature photoluminescence spectra of two intentionally undoped typical ZnS samples, ZnS154 and ZnS169, which were grown at lower and higher temperature, respectively. The Gaussian fit of the RT-PL spectrum for the ZnS154 sample shows a strong violet peak at 2.95 eV, two strong blue emission bands ~2.85 and ~2.65 eV, and a green emission band at 2.47 eV. Fig. 6b illustrates the Gaussian fit of the PL spectrum in the violet-blue-green-orange region for the ZnS169 sample, which shows a strong green emission at 2.32 with a shoulder at ~2.53 eV in the blue region, a deep level related orange emissions at ~2.10 eV as well as a weak UV band at ~3.27 eV. All the radiative emission bands observed in the present samples can be explained on the basis of the energy level diagram shown in Fig. 7, which is an adaptation of the one reported by Goswami and Sen [23]. The analysis is done considering the presence of defect levels due to oxygen ions

and interstitial sulphur ions in the system. The transition from oxygen trap levels to valence band in ZnS is reported to be in the UV region around 381 nm whereas the transition from the conduction band to the defect levels of interstitial sulphur ions is reported in the blue region around 440 nm [24]. The interstitial sulphur states marked as I_S in figure can act as deep acceptor levels.

One can comment on the intensity enhancement of the 2.64–3.2 eV range and specifically to the formation of distinct peaks at 2.65, 2.81 and 2.95 eV. In ZnS, the valence band consists largely of s and p orbitals from sulphur while the conduction band is mainly due to s -orbitals of zinc [25]. Although little is known about the energy levels of interstitial sulphur or zinc in ZnS, studies of the green luminescence of CdS powder suggest that interstitial Cd and S vacancies act as ‘shallow donors’ (electron traps) and interstitial S and Cd vacancies can behave as ‘deep acceptor’ (hole traps) [26]. If a similar band structure applies to powdered ZnS, the blue emission can be understood as follows.

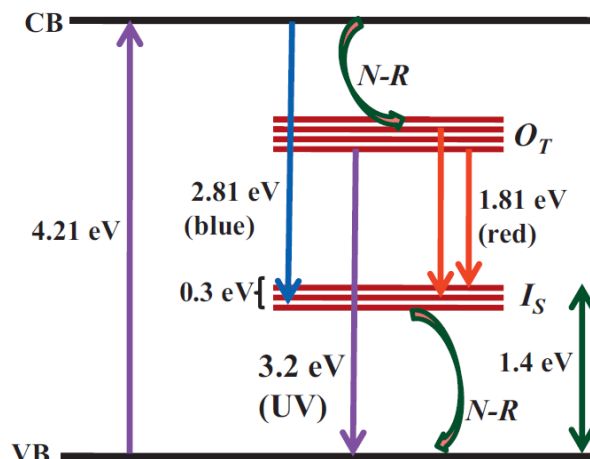


Fig. 7. Energy level diagram explaining the observed emission bands. VB: valence band, CB: conduction band, N-R: non-radiative transitions, O_T : oxygen trap levels, and I_S : interstitial sulphur states.

In Fig. 7 we illustrate the scheme of the energy states nanocrystalline ZnS band structure and the various processes involved during the PL of these materials. Sulphur vacancies in ZnS generate localized donor sites just below the conduction band. Excitation of these produce a positive charge and conduction band electrons. This localized charge exerts a potential, which can further trap electrons. So upon excitation, S^{2-} vacancies are pumping the electrons into conduction band. Emission occurs when a captured electron recombines with a hole in the valence band or in some acceptor level, which are interstitial sulphur states in this case. These emissions are similar to deep transitions, because here S^{2-} vacancies are behaving like impurity levels. Therefore, blue and violet emissions are attributed lattice defects related to sulphur and zinc vacancy or interstitials.

Figure 8 depicts the Raman spectra measured on the wurtzite-type ZnS films at 300 K. Before comparing the experimental results with previously reported data, one first presents an overview of the first-order Raman scattering from wurtzite ZnS. Wurtzite ZnS unit cell belongs to the C_{6v} point group symmetry with four atoms in a unit cell. The zone-

center optical phonons can be classified as the following irreducible representations: $\Gamma_{opt} = A_1 + E_1 + 2E_2 + 2B_1$. The B_1 modes are silent modes, A_1 and E_1 modes are polar modes and each splits into transverse-optical (TO) and longitudinal-optical (LO) components with different frequencies and both Raman and infrared active, and E_2 modes are nonpolar and Raman active only have two frequencies, the higher-frequency E_2 (high) mode is associated with the sulphur atoms and the lower-frequency E_2 (low) mode is associated with the vibration of the heavy Zn sublattice. The reported frequencies of the Raman active modes of wurtzite ZnS are shown in Table II. The Raman spectrum of sample ZnS154 mainly presents as dominant mode E_2 , which corresponds to E_2^2 and is observed around 285 cm^{-1} which confirms that the structure is wurtzite type [29]. As is observed the vibrational mode is dominant in this spectrum and is due to abundance of sulphur in the sample. As the growth temperature is increased the S molar fraction decreases appearing other peaks as E_2^1 at 68 cm^{-1} , which is associated with the vibration of the heavy Zn sublattice, as can be seen in Fig. 8.

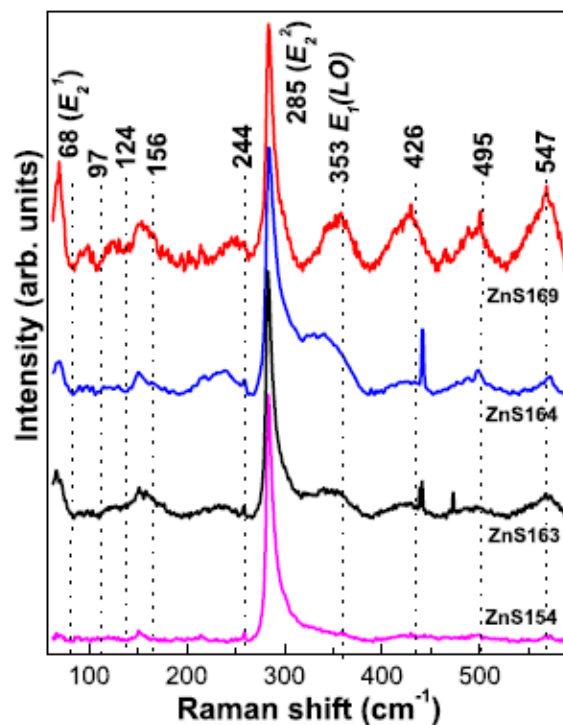


Fig. 8. Raman scattered spectra at 300 K from ZnS layers for different grown temperatures.

The optical phonon mode $A_1(LO) = E_1(LO)$ is reported to have the highest intensity in wurtzite ZnS structure, which was observed at 350 cm^{-1} . The relative intensity of this peak is a measure of the concentration of crystalline defects in the system. The intensity of the LO phonon mode is found to be comparable with that of the other optical modes in the present case. This is expected in view of the presence of defects in the system, as was inferred from luminescence studies. The LO phonon mode shows a red shift compared to the reported bulk value. Red shift of the LO phonon mode is known to occur in nanocrystalline systems due to spatial confinement as well as tensile stress due to the presence of defects [30]. Since PL studies indicate the presence of defects in the form of oxygen

trap ions and interstitial sulphur ions, the red shift observed here could be a combined effect of confinement as well as strain due to defects in the lattice.

TABLE II. FIRST-ORDER RAMAN FREQUENCIES OF EXPERIMENTAL AND THEORETICAL RESULTS FOR HEXAGONAL WURTZITE ZNS.

Phonon	Ref. [29]	Ref. [31]	Ref. [32]	Ref. [29]	This work
E_2^1		72	69	76	68
$A_1(TO)$	275	273	272	287	244
$E_1(TO)$	279	273	276	288	285
E_2^2	285	286	286	296	
$E_1(LO)$	353	351	351	347	350
$A_1(LO)$	353	351		350	

Brafman and Mitra have reported that the modes $A_1(TO)$ and $E_1(TO)$ occur at the same wave number 273 cm^{-1} [31]. However, Cheng et al. have calculated theoretically and later confirmed through experimental results that these modes can have different values [29]. The peak observed at 244 cm^{-1} in the present work is attributed to $A_1(TO)$ that is shifted to red. The composite peak near 166 cm^{-1} can be due to the overlap of peaks at 158 cm^{-1} and 177 cm^{-1} , attributed to two-phonon processes [31].

The selection rules for two-phonon Raman scattering in crystals with the wurtzite structure were reported by Siegle *et al.* [33]. The following general rules can be drawn. (i) Overtones always contain the representation A_1 while combinations belonging to different irreducible representations never contain A_1 . (ii) More overtones or combinations become allowed with decreasing symmetry of the point in the BZ considered. (iii) A consequence of the different packing sequence of wurtzite compared to zincblende is to have the BZ dimension in the cubic (111) direction, which is followed by folding of the phonon branches at the new zone boundary. It uses the phonon dispersion and the symmetry selection rules for two-phonon Raman scattering reported by Siegle *et al.* [40] to identify the second order features in the wurtzite ZnS Raman spectrum, as displayed in Fig. 9, which was obtained from ref. [33]. Accordingly, we can also divide the second order spectra of wurtzite ZnS into three regions: (i) the low frequency region (approximately $0\text{--}400 \text{ cm}^{-1}$) dominated by acoustic overtones, (ii) the high-frequency region ($540\text{--}600 \text{ cm}^{-1}$) formed by optical overtones and combinations, and (iii) the intermediate-frequency region ($400\text{--}540 \text{ cm}^{-1}$) where optical and acoustic phonon combinations occur.

In the low-frequency region (Fig. 8), there are five weak peaks at $78, 107, 134, 166$ and 254 cm^{-1} . The peak at 254 cm^{-1} is assigned to LA overtones along M-K, where phonon dispersion is nearly flat (see Fig. 9) and hence the DOS is very high. Above 380 cm^{-1} , we find the acoustic and optical combinations. For instance, the broad weak peak at 436 cm^{-1} can be assigned to $TA+LO$ at L point for flat phonon dispersion. The second-order Raman scattering in the high-frequency region corresponds to LO overtones and combinations involving LO modes. From Fig. 9, we find that the calculated frequencies derived from PDOS and multiplied by 2 shows one main broad band above 540 cm^{-1} which are

consistent with the measured Raman spectrum in this region.

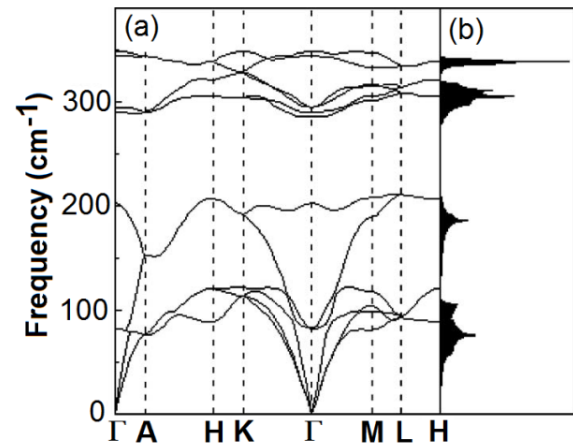


Fig. 9. (a) Phonons band structure and (b) PDOS of wurtzite ZnS, figure taken from ref. [33].

IV. CONCLUSION

The ZnS nanofilms grown by rf magnetron sputtering on GaAs (001) have been studied by XRD, SEM-EDS, room-temperature photoluminescence and. SEM shows that growth temperature can affect drastically the morphology of the nanofilms. XRD measurements show that the grain size remained almost constant ($\sim 29 \text{ nm}$) for the temperature range from 180 to 450°C . XRD analysis reveals that the sample grown at 180°C is polycrystalline and strongly textured, the samples from 270 to 450°C are polycrystalline with hexagonal phases, and the orientation for sample 630°C is believed to be influenced by the substrate orientation. ZnS/GaAs nanostructures thus produced exhibit different photoluminescent properties in the visible region as compared to their bulk counterpart.

REFERENCES

- [1] M. Tan, W. Cai, L. Zhang. Optical absorption of ZnS nanocrystals inside pores of silica. *Appl. Phys. Lett.* **71** (1997) 3697–3699.
- [2] W. Chen, Z. Wang, Z. Lin, L. Lin. Absorption and luminescence of the surface states in ZnS nanoparticles. *J. Appl. Phys.* **82** (1997) 3111–3115.
- [3] T. Yokogawa, T. Taguchi, Sh. Fujita, M. Satoh. Intense blue-emission band and the fabrication of blue light emitting diodes in I-doped and Ag-ion-implanted cubic ZnS. *IEEE Trans Electron Devices* **30** (1983) 271–7.
- [4] D. Theis, Selected Analytical Tools Yield a Better Insight into Electroluminescent Thin Films). *Phys. Stat. Sol. (a)*, **81**(1984) 647–655
- [5] J. Fang, P.H. Holloway, J.E. Yu, K.S. Jones, B. Pathangey, E. Brettschneider, T.J. Anderson. MOCVD growth of non-epitaxial and epitaxial ZnS thin films. *Appl. Surf. Sci.* **70/71** (1993) 701–706.
- [6] K. T. Tran, W. Park, W. Tong, M. M. Kyi, K. B. Wagner, J. C. Summers. Photoluminescence properties of ZnS epilayers. *J. Appl. Phys.* **81** (1997) 2803–2809.
- [7] G. Shimaoka, T. Arakawa, Y. Suzuki. Electron induced epitaxy of cubic ZnS on GaAs (100) surfaces. *Appl. Surf. Sci.* **212/213** (2003) 694–700.
- [8] B. Greengerg, K. W. Zwickler, I. Cadoff. ZnSepitaxy on sapphire {110}. *Thin Solid Films* **141** (1986) 89–97.
- [9] J. W. Cook Jr, B. D. Eason, P. R. Vaudo, F. J. Schetzina. Molecular-beam epitaxy of ZnS using an elemental S source. *J. Vac. Sci. Technol.* **B10** (1992) 901–904.

- [10] J. Ihanus, M. Ritala, M. Leskelä, T. Prohaska, R. Resch, G. Friedbacher, M. Grasserbauer. AFM studies on ZnS thin films grown by atomic layer epitaxy. *Appl. Surf. Sci.* **120** (1997) 43–50.
- [11] C. W. Wang, T. J. Sheu, Y. K. Su, M. Yokoyama. The study of aging mechanism in ZnS: Mn thin-film electroluminescent devices grown by MOCVD. *Appl. Surf. Sci.* **113/114** (1997) 709–713.
- [12] P. Prete, N. Lovergine, M. Masser, C. Zanotti-Fregonora, A. M. Mancini. Diethylsulphide as sulphur precursor for the low temperature metalorganic vapour-phase epitaxy of ZnS: growth, morphology and cathodoluminescence. *J. Cryst. Growth* **204** (1999) 29–34.
- [13] T. K. Hillie, C. Current, H. C. Swart. ZnS thin films grown on Si (100) by XeCl pulsed laser ablation. *Appl. Surf. Sci.* **177** (2001) 73–77.
- [14] N. Kumbhojkar, V. V. Nikesh, A. Kshirsagar, S. Mahamuni. Photophysical properties of ZnS nanoclusters. *J. Appl. Phys.* **88**(2000) 6260-6264.
- [15] B. Salazar-Hernández, M. A. Vidal, H. Navarro-Contreras, R. Asomoza, A. Merkulov. Excitonic transitions in $(\text{GaAs})_{1-x}(\text{Ge}_2)_x/\text{GaAs}$ multilayers grown by magnetron sputtering. *Appl. Phys. Lett.* **72** (1998) 94–96.
- [16] S. F. Chichibu, T. Yoshida, T. Onuma, H. Nakanishi. Helicon-wave-excited-plasma sputtering epitaxy of ZnO on sapphire (0001) substrates. *J. Appl. Phys.* **91** (2002) 874–877.
- [17] A. Boudghene-Stambouli, S. Hamzaoui, M. Bouderbala. Blue emitting ACPEL devices based upon ZnS:TM, Li. *Thin Solid Films* **283** (1996) 204–208.
- [18] K. Hideki, Y. Yoji, M. Yukinoro, T. Yukihisa. ZnS: Mn thin films electroluminescent devices prepared by metalorganic chemical vapor deposition. *J. Cryst. Growth* **169** (1996) 33–39.
- [19] B. E. Warren. X-Ray diffraction. New York: Dover; 1990.
- [20] S. Radhu, C. Vijayan. Observation of red emission in wurtzite ZnS nanoparticles and the investigation of phonon modes by Raman spectroscopy. *Mater. Chem. Phys.* **129** (2011) 1132–1137.
- [21] W.Q. Peng, G.W. Cong, S.C. Qu, Z. G. Wang. Synthesis of shuttle-like ZnO nanostructures from precursor ZnS nanoparticles. *Nanotechnology* **16** (2005) 1469-1473.
- [22] X.D. Gao, X.M. Li, W. D. Yu. Structure and UV photoluminescence of nanocrystalline ZnO films prepared by thermal oxidation of ZnS films. *Mater. Sci. Eng. B* **113** (2004) 274-278.
- [23] N. Goswami, P. Sen. Photoluminescent properties of ZnS nanoparticles prepared by electroexplosion of Zn Wires. *J. Nanopart. Res.* **9** (2007) 513-517.
- [24] V.N. Do, N.T. Tuan, D.Q. Trung, N.D. Kien, N.D. Chien, P. T. Huy. One-dimensional fabricated by oxidizing ZnS nanowires. *Mater. Lett.* **64** (2010) 1650-1652.
- [25] D. Curie, 1963. Luminescence in crystals (Methuen, London, chapters 4 and 5).
- [26] I. Uchida. Green Edge Emission in CdS. *J. Phys. Soc. Jpn.* **21** (1966) 645-649.
- [27] K. Vanheusden, W.L. Warren, C.H. Seager, D.R. Tallant, J. A. Voigt. Mechanisms behind green photoluminescence in ZnO phosphor powders. *J. Appl. Phys.* **79**(1996) 7983-7990.
- [28] Y.W. Heo, D.P. Norton, S. J. Pearton. Origin of green luminescence in ZnO thin film grown by molecular-beam epitaxy. *J. Appl. Phys.* **98**(2005) 073502.
- [29] Y. C. Cheng, C. Q. Jin, F. Gao, X. L. Wu, W. Zhong, S. H. Li, Paul K. Chu. Raman scattering study of zinc blende and wurtzite ZnS. *J. Appl. Phys.* **106** (2009) 123505.
- [30] A. Tanaka, O. Seinosuke, T. Arai. Low-frequency Raman scattering from CdS microcrystals embedded in a germanium dioxide glass matrix. *Phys. Rev.* **B47** (1993) 1237-1243.
- [31] O. Brafman, S. S. Mitra. Raman Effect in Wurtzite- and Zinc-Blende-Type ZnS Single Crystals. *Phys. Rev.* **171** (1968) 931-934.
- [32] J. Schneider, R. D. Kirby. Raman Scattering from ZnS Polytypes. *Phys. Rev.* **B6** (1972) 1290-1294.
- [33] H. Siegle, G. Kaczmarczyk, L. Filippidis, A. P. Litvinchuk, A. Hoffmann, C. Thomsen. Zone-boundary phonons in hexagonal and cubic GaN. *Phys. Rev. B* **55**(1997) 7000-7004.